A Permian Layered Intrusive Complex in the Western Tarim Block, Northwestern China: Product of a Ca. 275-Ma Mantle Plume?

Chuan-Lin Zhang,[1] *Xian-Hua Li,*[2] *Zheng-Xiang Li,*[3] *Hai-Min Ye,*[4] *and Chang-Nian Li*[5]

Key Laboratory of Isotope Geochronology and Geochemistry, Guangzhou Institute of Geochemistry, Chinese Academy of Sciences, Guangzhou 510640, China
(e-mail: zchuanlin@yahoo.com.cn)

ABSTRACT

Zircon laser ablation inductively coupled plasma mass spectrometry U-Pb age and geochemical and Sr-Nd-Hf isotopic data are reported for the Bachu layered intrusive complex (BLIC) in the western Tarim Block and are used to assess the possible presence of a Permian large igneous province (LIP) in the region. The BLIC intrudes the Silurian-Devonian sedimentary rocks, and our U-Pb zircon dating gives a crystallization age of 274 ± 2 Ma. Rock types of the BLIC include pyroxenite, diorite, syenite, and quartz syenite, with a wide range of SiO_2 contents (38.6%–68.7%) and variably high alkalinity ($Na_2O + K_2O$ = 1.5%–12.0%, K_2O/Na_2O = 0.23–0.9). They are enriched in Rb, Ba, Th, Nb, Ta, Zr, Hf, and light rare earth elements. Isotopically, they are characterized by positive whole-rock $\varepsilon Nd(t)$ values (0.25–2.8, mostly above 2.0) and zircon $\varepsilon Hf(t)$ values (5.8–8.9) and low initial $^{87}Sr/^{86}Sr$ ratios (0.7035–0.7045). These features suggest that the BLIC was likely formed by crystal cumulation and fractionation (with negligible crustal contamination) of alkali basalts derived from an ocean island basalt–like mantle source (i.e., the asthenospheric mantle) in an extensional regime. We suggest that these mid-Permian igneous rocks, in combination with the voluminous coeval basalts and intrusive rocks covering an total area of ca. 250,000 km^2 in the Tarim Block and surrounding regions, constitute an LIP (the "Bachu LIP") and that the BLIC could be the residue of a feeder for this LIP.

Online enhancements: appendix tables, color version of figure 1.

Introduction

Although alkaline rocks are volumetrically insignificant, their petrogenesis is controversial because of their peculiar chemical compositions, exotic mineralogy, and tectonic associations. Alkaline rocks can occur in all settings except mid-oceanic ridges (Zhao et al. 1995; Farmer 2003), and a number of petrogenetic models have been suggested for their genesis, such as partial melting of a metasomatized mantle enriched in light rare earth elements (LREEs) and large-ion lithophile elements (LILEs; Dawson 1987; Edgar 1987; Yang et al. 2005*b*; Upadhyay et al. 2006*a*), low-degree partial melting of an asthenospheric mantle with subsequent crystal fractionation (Fitton 1987; Bailey et al. 2001, 2006), interaction of an asthenospheric melt with the lithospheric mantle (Menzies 1987; Baker et al. 1997), partial melting of crustal rocks resulting from an influx of volatiles (Lubala et al. 1994; Martin 2006) or in a closed system at pressures typical of the base of an overthickened crust (Huang and Wyllie 1981), and magma mixing of mantle-derived basaltic and crust-derived silicic melts followed by differentiation of the hybrid liquid (Dorais 1990; Zhao et al. 1995; Litvinovsky et al. 2002). These distinct petrogenetic models partly reflect the diversity of geological settings in which the alkaline rocks occur.

We present here results of a detailed petrographic,

Manuscript received August 20, 2007; accepted February 13, 2008.

[1] Author for correspondence; present address: Nanjing Institute of Geology and Mineral Resources, Nanjing 210016, China.
[2] State Key Laboratory of Lithospheric Evolution, Institute of Geology and Geophysics, Chinese Academy of Sciences, Beijing 100029, China.
[3] Department of Applied Geology, Institute for Geoscience Research, Curtin University of Technology, GPO Box U1987, Perth, Western Australia 6845, Australia.
[4] Nanjing Institute of Geology and Mineral Resources, Nanjing 210016, China.
[5] Department of Earth Sciences, Chinese University of Geosciences, Wuhan 430074, China.

[The Journal of Geology, 2008, volume 116, p. 269–287] 0022-1376/2008/11603-0002$15.00 DOI: 10.1086/587726

geochemical, and geochronological study of rocks from the Bachu alkaline layered intrusive complex (BLIC) in the northwestern Tarim Block, China (fig. 1). The aim of the study is to constrain the timing of the emplacement and to reconstruct the petrogenetic evolution and geodynamic setting of this complex and related igneous rocks by synthesizing field, petrographic, geochronological, elemental, and whole-rock Sr-Nd and zircon Hf isotopic data.

General Geology and Petrography

The Tarim Block, located in northwestern China, amalgamated with the southern Central Asian Orogenic Belt (CAOB) during the Late Paleozoic (fig. 1*a*; Xinjiang BGMR 1993, p. 17–45; Li 2006). Late Carboniferous to Permian intrusive complexes, mafic dikes, and a large volume of volcanic rocks have been reported recently both within the Tarim Block (e.g., Jia 1997; Jiang et al. 2004*a*, 2004*b*; Xu et al. 2005; Yang et al. 2007) and along its northern fringes (mainly in the Tienshan area to the north of Tarim but also in the Baikal area; e.g., Pisarevsky et al. 2006). Several models have been proposed for the geodynamic settings of those Late Carboniferous to Permian igneous rocks. (1) Considering the Tarim Block to have amalgamated with the Muyunk Block along the central Tienshan suture zone in the Early Carboniferous (Li 2006), Xu et al. (2005) argued that the Late Carboniferous to Permian voluminous A-type granites and Permian mafic igneous rocks were genetically related to the postorogenic collapse. Zhou et al. (2006) also used this model to explain the formation of the Permian basalts in Santanghu and Tuha basins north of Tienshan (fig. 1*a*). (2) Yang et al. (1995, 2005*b*, 2006*a*) suggested that those igneous rocks could be the products of the northward subduction of the paleo-Tethyan oceanic crust between the Eurasian continent to the north and the Gondwanan continents to the south. (3) From the estimated high Mg# (~73) of the primary magma for the ca. 270-Ma ultramafic intrusions in eastern Tienshan, Zhou et al. (2004) argued that a Permian mantle plume could account for the formation of those mafic rocks, the voluminous A-type granites in Tienshan, and the late Paleozoic crustal growth in the CAOB. Other researchers (e.g., Jiang et al. 2001, 2004*a*, 2004*b*; Chen et al. 1999; Yang et al. 2007) reported work on Permian igneous rocks and lithofacies paleogeography of the Tarim Block that indicates extensional tectonic regimes.

The BLIC, studied here, outcrops ca. 12 km southeast of Bachu County (fig. 1) in the Tarim Block interior. Field observations show that the complex is an oval-shaped (see the topographic inset at the lower right-hand corner of fig. 1*a*), layered intrusion with ca. 12 km^2 of outcropping area. It consists of ultramafic-mafic-felsic rocks that intrude Silurian-Devonian sedimentary rocks, with contact zones dipping 20°–40° toward the interior of the complex (figs. 1*b*, 2). On the basis of thin-section examinations and field observations, as well as previous petrographic studies (Li et al. 2001), we divide the complex into four main lithofacies: (1) magnetite-olivine-pyroxenite (accounting for ~5% of the outcrop), (2) (olivine-bearing) pyroxenite (~30%), (3) gabbro (~60%), and (4) syenite and quartz syenite (~5%; fig. 1*b*). Transitional rock types, for example, pyroxene-bearing diorite, olivine-bearing gabbro, pyroxene, and/or nepheline-bearing syenite, also exist within the BLIC. Thus, the BLIC includes rocks ranging from ultramafic, mafic, and intermediate to felsic types, although the intermediate types are volumetrically insignificant. All the rocks are relatively fresh, with only slight metasomatism, as represented by sericite as a replacement for plagioclase. They show clear medium- to coarse-grained texture and a block structure.

The magnetite-olivine-pyroxenite lithofacies is composed mainly of olivine (10%–20%), augite (40%–50%), plagioclase (10%–20%), magnetite (10%–30%), and minor amounts of phlogopite (~1%) and apatite (<1%). In augite, glint texture (where spiculate titanium and iron oxide are parallel to the cleavage of augite) is visible. The pyroxenite lithofacies is composed mainly of clinopyroxene (75%–95%), with minor amounts of olivine, plagioclase, and Ti-Fe oxides. Gabbro, the predominant lithofacies of the complex, consists of clinopyroxene (40%–50%), plagioclase (40%–45%), and minor amounts of hornblende, phlogopite, and apatite. Orbicular structures with dimensions of ~50 cm × 50 cm were observed on several outcrops in this lithofacies. The quartz-syenite lithofacies is exposed in a topographic high near the center of the complex (figs. 1, 2). The main minerals are alkaline feldspar (orthoclase, 40%–70%), quartz (10%–30%), hornblende (5%–10%), and brown biotite (1%–2%); the accessory minerals include zircon, apatite, rutile, allanite, and monazite. On several outcrops, minor nepheline-bearing syenite was also observed (such as sample Wp-63). The nepheline-bearing syenite consists of alkaline feldspar (40%–60%), pyroxene (40%–50%), nepheline (1%–5%), and phlogopite (1%–5%) as well as accessory minerals, such as apatite, allanite, xenotime, and baddeleyite.

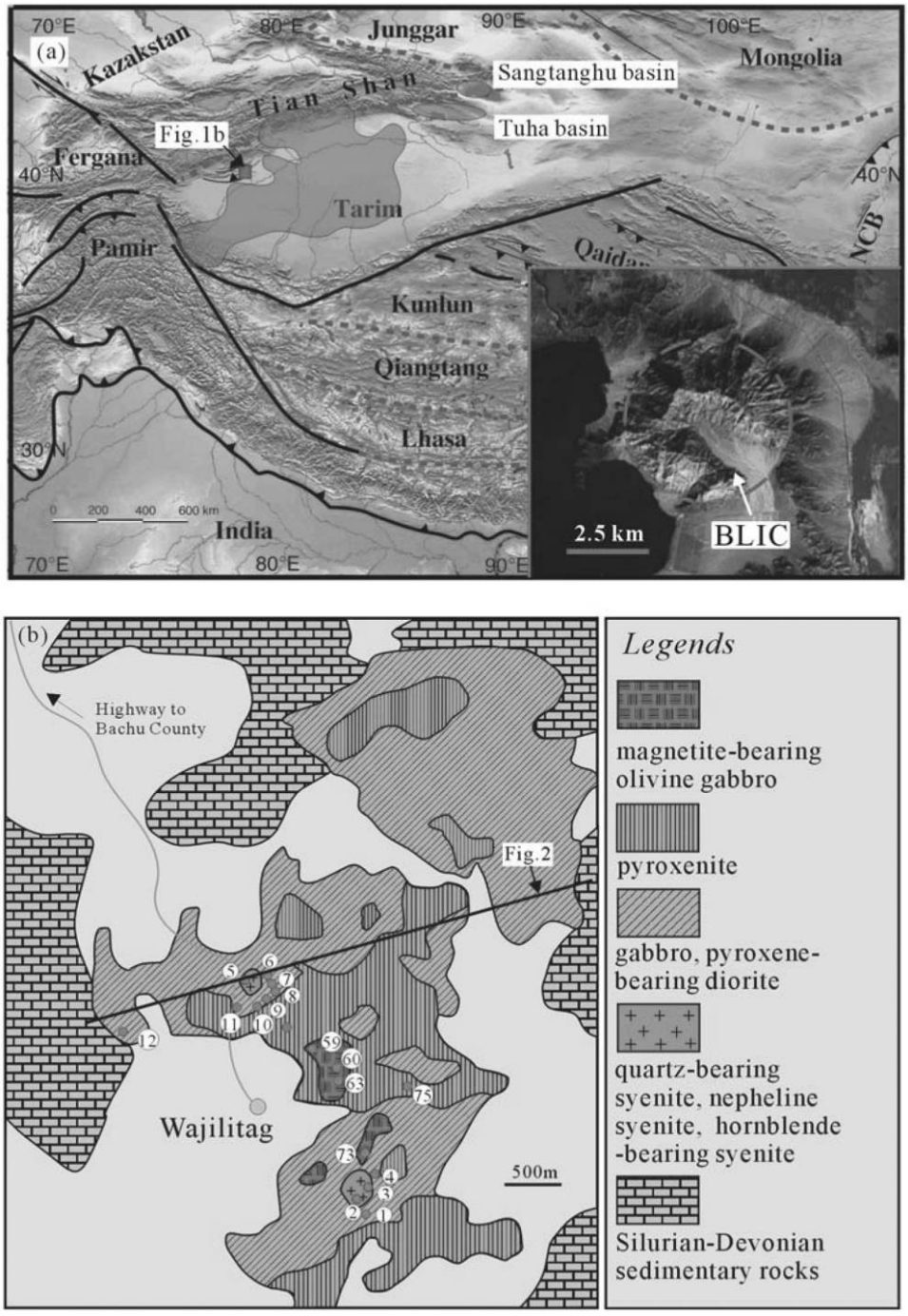

Figure 1. *a*, Topographic and simplified tectonic map of the Tarim Block and its surrounding regions, showing the distribution of Permian basalts in Tarim and the location of the Bachu layered ultramafic-mafic-syenite complex (*BLIC*, inset). Coeval basalts in the Tuha and Sangtanghu basins are also shown. Solid and dashed lines indicate active faults and ancient sutures, respectively (after Chen et al. 2004). *b*, Geological map of the BLIC. The sample locations are shown, with the numbers representing samples listed in table A2, available in the online edition or from the *Journal of Geology* office; that is, 1–12 correspond to samples 05BH-1–05BH-12, and 59–75 correspond to samples Wp-59–Wp-75. *NCB* = North China Block.

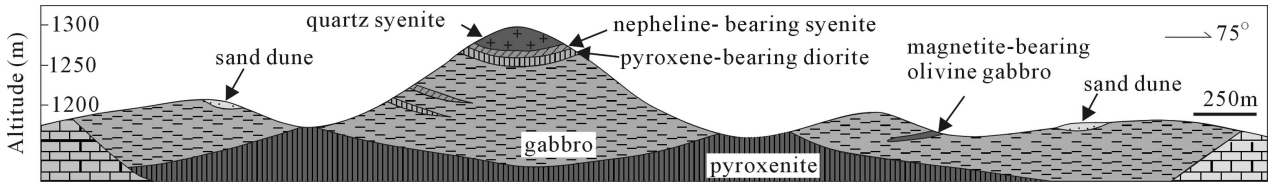

Figure 2. Schematic geological section showing the layered structure of the Bachu complex, simplified from Li et al. (2001), with minor modification made based on our field observations.

Analytical Methods

A quartz-syenite sample (BC03) was collected from the felsic lithofacies in the BLIC (78°48′25″E, 39°45′2″N) for zircon U-Pb and Hf isotope analyses. Mineral separation was carried out; first, conventional magnetic and density techniques were used to concentrate the nonmagnetic, heavy fractions. A representative selection of zircons was then extracted by handpicking under a binocular microscope. Zircon grains, with TEMORA standard (417 Ma), were cast into an epoxy mount, which was then polished to section the crystals for analysis. Zircons were documented with transmitted- and reflected-light micrographs, as well as cathodoluminescence (CL) images, to allow the study of their inner structures. Zircons were dated in situ on an excimer (193-nm wavelength) laser ablation inductively coupled plasma mass spectrometer (LA-ICP-MS) at the State Key Laboratory of Continental Dynamics, Northwest University, China. The ICP-MS used was an Agilent 7500a (with shield torch), and the GeoLas 200M laser ablation system (MicroLas, Göttingen, Germany) was used for the laser ablation experiments. Analytical processes were similar to those described by Yuan et al. (2004). Raw count rates were measured for ^{29}Si, ^{204}Pb, ^{206}Pb, ^{207}Pb, ^{208}Pb, ^{232}Th, and ^{238}U. U, Th, and Pb concentrations were calibrated by using ^{29}Si as an internal standard and NIST SRM 610 as the reference standard. $^{207}Pb/^{206}Pb$, $^{206}Pb/^{238}U$, $^{207}Pb/^{235}U$, and $^{208}Pb/^{232}Th$ ratios, calculated using GLITTER 4.0 (Macquarie University, Sydney, Australia), were corrected for both instrumental mass bias and elemental and isotopic fractionation by using standard zircon 91500 (Wiedenbeck et al. 1995) as external standard. The ages were calculated with ISOPLOT 3.0 (Ludwig 2003). Our three measurements of TEMORA as an unknown yielded a weighted mean $^{206}Pb/^{238}U$ age of 417 ± 9 Ma, which is in good agreement with the recommended isotope dilution–thermal ionization mass spectrometry (ID-TIMS) age of 416.75 ± 0.24 Ma (Black et al. 2003). U-Pb zircon results are listed in table A1, available in the online edition or from the *Journal of Geology* office.

Major-element, trace-element, and Nd isotope measurements were carried out at the Guangzhou Institute of Geochemistry, Chinese Academy of Sciences. Major elements were analyzed by x-ray fluorescence (Rigaku ZSX100e) according to the analytical procedures of Li et al. (2005). Analytical precision was generally better than 2%. Trace elements were analyzed with a Perkin-Elmer Sciex ELAN 6000 ICP-MS according to procedures described by Li et al. (2002). Powdered samples of ~50 mg were dissolved in high-pressure Teflon bombs using a HF + HNO_3 mixture. An internal standard solution containing the single element Rh was used to monitor signal drift during ion counting. The USGS standards BCR-1, W-2, and G-2 and the Chinese National standards GSR-1 and GSR-3 were used for calibrating element concentrations of measured samples. In-run analytical precision for most elements was better than 3%–5%. The analytical results for major and trace elements are listed in table A2, available in the online edition or from the *Journal of Geology* office.

Nd isotopes were determined by using a Micromass Isoprobe multicollector ICP-MS (MC-ICP-MS) according to the procedure described by Li et al. (2004). Sr isotopes were measured with a Finnigan MAT 262 thermal ionization mass spectrometer at the Institute of Geology and Geophysics, Chinese Academy of Sciences, according to the procedure described by Wu et al. (2005). Measured $^{87}Sr/^{86}Sr$ and $^{143}Nd/^{144}Nd$ ratios were normalized to $^{86}Sr/^{88}Sr = 0.1194$ and $^{146}Nd/^{144}Nd = 0.7219$, respectively. The reported $^{87}Sr/^{86}Sr$ and $^{143}Nd/^{144}Nd$ ratios were adjusted to the NBS SRM 987 standard $^{87}Sr/^{86}Sr = 0.71025$ and the Shin Etsu JNdi-1 standard $^{143}Nd/^{144}Nd = 0.512115$. Sr-Nd isotope results are listed in table 1. In situ zircon Hf isotopic analysis was carried out on a Neptune MC-ICP-MS equipped with a Geolas-193 laser ablation system (LAM-MC-ICP-MS) at the Institute of Geology and Geophysics, Chinese Academy of Sciences. The de-

Table 1. Nd-Sr Isotope Compositions of Rocks from the Bachu Layered Intrusive Complex

Sample	Sm (ppm)	Nd (ppm)	$^{147}Sm/^{144}Nd$	$^{143}Nd/^{144}Nd \pm 2\delta$	T_{DM}[a] (Ma)	$\varepsilon Nd(t)$	Rb (ppm)	Sr (ppm)	$^{87}Rb/^{86}Sr$	$^{87}Sr/^{86}Sr \pm 2\delta$	$(^{87}Sr/^{86}Sr)_i$[b]
05BH-1	6.71	41.1	.1034	.512595 ± .000007	790	2.38	56.0	639	.212	.757022 ± .000012	.70393
05BH-3	11.1	58.0	.1218	.512573 ± .000008	760	2.41	94.0	24.6	9.245	.709789 ± .000011	.73177
05BH-4	11.2	67.0	.1062	.512620 ± .000008	940	1.34	84.8	170	1.204	.727986 ± .000013	.70650
05BH-5	23.6	139	.1078	.512587 ± .000007	740	2.80	144	78.8	4.410	.705027 ± .000012	.71594
05BH-6	11.9	67.9	.1115	.512601 ± .000006	800	2.11	66.3	599	.267	.704820 ± .000011	.70429
05BH-7	8.77	47.8	.1163	.512613 ± .000006	810	2.25	62.4	525	.287	.704323 ± .000012	.70403
05BH-9	14.0	80.9	.1101	.512605 ± .000007	830	2.31	88.7	735	.291	.704873 ± .000011	.70352
05BH-10	11.0	61.0	.1142	.512559 ± .000005	890	1.34	50.2	776	.156	.703796 ± .000011	.70444
05BH-12	24.5	124	.1251	.512523 ± .000012	1050	.25	24.2	811	.072	.757022 ± .000012	.70359

[a] Model age.
[b] Initial $^{87}Sr/^{86}Sr$.

tailed analytical procedures are given by Wu et al. (2006) and Yang et al. (2006*b*). Hf isotopic analyses were obtained on 30 zircons, including 16 zircons dated at ~274 Ma by SHRIMP and 14 undated zircons that share similar CL image features to those ca. 274-Ma zircons. Zircon Hf isotopic results are listed in table A3, available in the online edition or from the *Journal of Geology* office.

Results

U-Pb Zircon Age. Zircon grains from sample BC03 are mostly euhedral, transparent, colorless, and 200–300 μm long, with length-to-width ratios of 2–3. Euhedral concentric zoning is common in most crystals under CL images, typical of magmatic origin. Relict cores were not observed. Analyses were conducted on 20 zircon grains (table A1). U concentrations ranged from 68 to 225 ppm, Th concentrations from 36 to 115 ppm, and Th/U ratios from 0.42 to 0.62. Among the 20 analyses, two analyses (spots 14.1 and 15.1) have relatively older concordant $^{206}Pb/^{238}U$ and $^{207}Pb/^{235}U$ ages, and another two (spots 13.1 and 16.1) have apparent radiogenic-Pb loss (fig. 2). These are likely to be inherited or (more likely) captured zircons (e.g., in CL images, these four zircon grains have melting dents on their rims). In the $^{206}Pb/^{238}U$-$^{207}Pb/^{235}U$ concordia plot, the remaining 16 analyses are concordant within errors (fig. 3), yielding a weighted mean $^{206}Pb/^{238}U$ age of 274 ± 2 Ma (MSWD = 2.4). This age is interpreted as the timing of the BLIC emplacement. It is noted that this emplacement age is identical with a zircon SHRIMP U-Pb age of 272 ± 1.2 Ma for a quartz syenite dike and a whole-rock Sm-Nd isochron age of 259 ± 57 Ma for a mafic dike south of the BLIC (Yang et al. 2006*a*) and is close to a $^{40}Ar/^{39}Ar$ plateau age of 278.5 ± 1.4 Ma for the Permian basalts in central Tarim (Chen et al. 1997; Jia 1997).

Geochemistry. *Major and Trace Elements.* The BLIC rocks show distinct alkaline affinities ($Na_2O + K_2O$ = 1.5%–12.0%) over a large range of SiO_2 contents (38.5%–68.7%; fig. 4). The agpaitic index ($[(Na_2O+K_2O)/Al_2O_3]_{molar}$) values of 0.4–0.97 (mostly above 0.6) mirror those of miaskitic mineralogy, and the K_2O/Na_2O ratios of 0.23–0.9 (with the exception of sample Wp-59, which has a high K_2O/Na_2O ratio of 1.14, possibly as a result of deuteric alterations) give them sodic affinities.

According to major-element compositions, the rocks could be subdivided into three subgroups: ultramafic-mafic (SiO_2 = 38.6%–51.3%), intermediate (SiO_2 = 56.2%–64.0%), and silicic (SiO_2 = 67.9–68.7%; fig. 4). Major-element concentrations show a large variation in the complex due to crystal accumulation and fractionation, as indicated by (1) a decrease in TiO_2, CaO, and Fe_2O_3(T) and an increase in SiO_2, Al_2O_3, and K_2O with decreasing MgO, and (2) variations in P_2O_5 contents, where the felsic rocks have much lower values than the mafic-ultramafic and intermediate rocks (fig. 5).

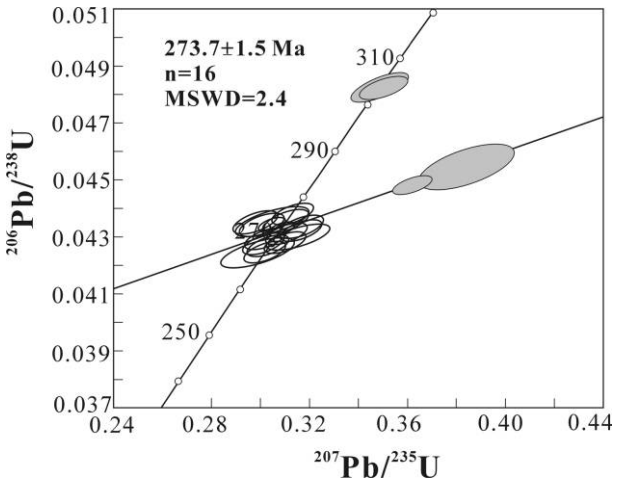

Figure 3. U-Pb zircon concordia diagram for the quartz-syenite in the Bachu intrusive complex. The concordant age of 273.7 ± 1.5 Ma is interpreted as the crystallization age of the intrusive complex.

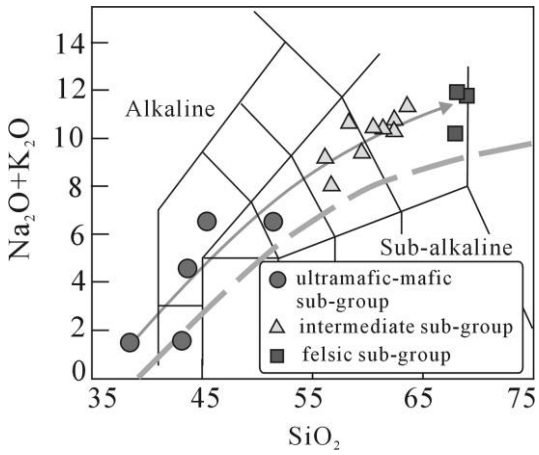

Figure 4. SiO_2 versus K_2O + Na_2O classification diagram, showing the alkaline characteristics of all the rocks from the Bachu layered intrusive complex.

Moreover, the mafic-ultramafic members of the complex show more scatter in the trends of oxides, which may be due to the presence of cumulus crystals of oxides, olivine, and pyroxene, as observed in thin sections. The ultramafic-mafic subgroup, with normative nepheline, represents a silica-undersaturated suite of rocks, whereas the intermediate and felsic subgroups are silica saturated (except for sample Wp-63, which contains minor nepheline). Most analyzed samples had low abundances of compatible elements such as Ni, Cr, Sc, and Co (table A2), indicating evolved compositions.

Figure 6*a* shows the compositions of the intermediate and felsic rocks in terms of their molar ratios of $Al_2O_3/(CaO + K_2O + Na_2O)$ (A/CNK) and $Al_2O_3/(Na_2O + K_2O)$ (A/NK). On the basis of these ratios, the intermediate rocks are metaluminous, whereas the felsic rocks straddle the metaluminous-peraluminous boundary. High concentrations of Zr, Nb, Ce, and Y and high Nb/Y and Fe/Mg (molar) ratios distinguish those Si-saturated rocks from I- and S-type granites. They are affinitive to A-type granites on the 10,000Ga/Al versus Zr discrimination diagram (fig. 6*b*; Winchester and Floyd 1977; Whalen et al. 1987; Frimmel et al. 2001), resembling the A_1 subtype as defined by Eby (1992) in terms of their high Nb, Y, and Ce contents (fig. 6*c*). Chemical compositions of the five syenite dike samples reported by Yang et al. (2006*a*) are also plotted in figure 6. Considering their similar major- and trace-element compositions, we suggest that the syenite dikes and the BLIC syenites share a common magma source.

The chondrite-normalized REE patterns of the ultramafic-mafic subgroup show LREE enrichments with steep slopes (La_N/Yb_N = 12–31) and insignificant Eu anomalies (fig. 7*a*; after Sun and McDonough 1989). The abundances of LILEs, such as Rb, Ba, and Sr, and high-field-strength elements (HFSEs), such as Zr, Hf, Nb, and Ta, of the ultramafic-mafic subgroup also exhibit large variation due to crystal fractionation and cumulation (fig. 7*b*; after Sun and McDonough 1989). The intermediate-subgroup samples have relatively coherent trace-elemental compositions exhibiting similar REE and trace-element distribution patterns (fig. 7*c*, 7*d*), except for a positive Eu anomaly for three samples (05BC-1, 6, and 10), and variable negative anomalies of Sr, P, and Ti in the trace-element distribution patterns. The felsic subgroup rocks (quartz syenite) have very variable total REE contents (206–775 ppm) and other trace-element contents. However, they have coherent left-sloping REE and trace-element distribution patterns (fig. 7*e*, 7*f*). They are enriched in LREEs, with $(La/Yb)_N$ ranging from 14 to 19, and have significant negative Eu anomalies (δEu = 0.4–0.5) and pronounced negative Sr, P, and Ti anomalies in trace-element distribution patterns.

Whole-Rock Nd-Sr and Zircon Hf Isotope Compositions. Sm-Nd isotopic data are presented, along with their Nd model ages (T_{DM}) and εNd(t) values calculated using the same formulation as in Li et al. (2003), assuming a depleted-mantle source with present-day $^{143}Nd/^{144}Nd$ = 0.51315 and $^{147}Sm/^{144}Nd$ = 0.2137 (table 1). The BLIC samples have variable Sm and Nd contents but relatively constant $^{147}Sm/^{144}Nd$ and $^{143}Nd/^{144}Nd$ ratios ranging from 0.1034 to 0.1251 and 0.512505 to 0.512620, respectively, corresponding to εNd(t) values of 0.25–2.8 (mostly above 2.0) and T_{DM}'s of 740–1050 Ma. Sample 05BH-12, which was collected at the fringe of the BLIC (fig. 1*b*), has the lowest εNd(t) value, 0.25, and significant Nb-Ta and Zr-Hf troughs in trace-element distribution patterns (fig. 6). These features were probably due to crustal assimilation. However, crustal assimilation, if any (such as presence of zircon xenocrysts in sample 05BC03), seems insignificant for other BLIC samples because they exhibit relatively high εNd(t) values (>2) and high Nb/La ratios of ~1.0.

Among the nine analyzed samples, three have high $^{87}Rb/^{86}Sr$ ratios of between 1.2 and 9.2 as a result of crystal fractionation (Jahn et al. 2001). Their very high $(^{87}Sr/^{86}Sr)_i$ ratios (where "i" indicates "initial") are only mean values, because the high $^{87}Rb/^{86}Sr$ ratios would produce large uncertainties in the calculated $(^{87}Sr/^{86}Sr)_i$ (Jahn et al.

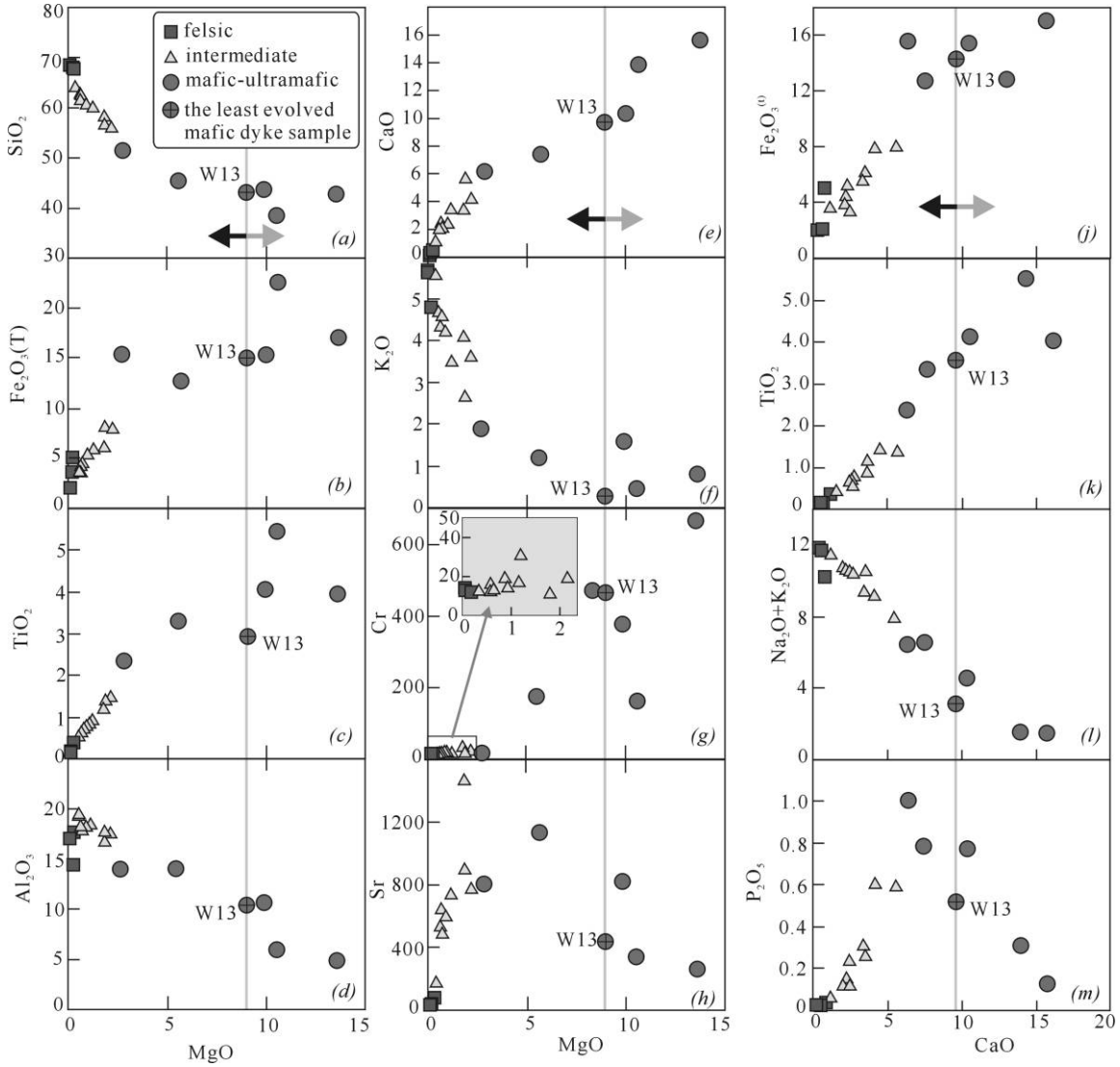

Figure 5. Binary Harker diagrams (MgO vs. SiO_2, Fe_2O_3(T), TiO_2, Al_2O_3, CaO, K_2O, Cr, and Sr; CaO vs. Fe_2O_3, TiO_2, $Na_2O + K_2O$, and P_2O_5) for the rocks from the Bachu intrusive complex, northwestern China. The trend and scattering suggest that cumulus and fractional processes produced most of the geochemical variations (symbols as in fig. 4). The least evolved mafic dike sample, W13 (Jiang et al. 2004*a*), is regarded as representing the most primitive magma of the Bachu layered intrusive complex. The black and gray arrows indicate crystal fractionation and cumulation, respectively (see details in "Petrogenesis").

2000*b*). The other six samples have low $^{87}Rb/^{86}Sr$ (0.0722–0.2912) and relatively homogeneous $(^{87}Sr/^{86}Sr)_i$ ratios of between 0.70352 and 0.70444. These samples define a narrow cluster on the Sr-Nd diagram (fig. 8), indicating that they were derived from a homogenous mantle source.

Zircon Hf isotopic data show that all zircons have very low $^{176}Lu/^{177}Hf$ ratios of <0.0012 and relatively homogeneous $^{176}Hf/^{177}Hf$ ratios (0.282755–0.282867, with an average of 0.282822). The calculated $\varepsilon Hf(t)$ values range from 5.3 to 8.8, with an average of 7.8 ± 1.3. Such highly positive $\varepsilon Hf(t)$ values suggest crystallization of zircons from mantle-derived melts, consistent with the whole-rock Sr-Nd isotopic data.

Petrogenesis

Trace-Element and Isotopic Constraints on the Source Region. Because the ultramafic-mafic rocks account for more than 90% volume of the whole complex (estimated according to their outcropping

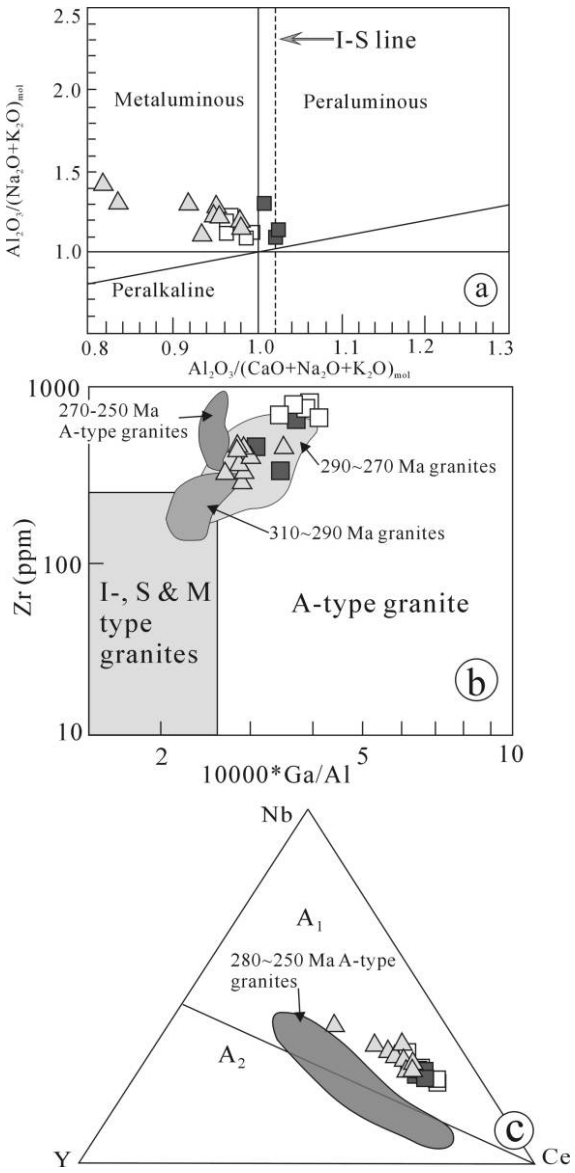

Figure 6. *a*, A/NK versus A/CNK plot showing that the intermediate subgroup from the Bachu layered intrusive complex (BLIC) are metaluminous and that the felsic subgroup straddles the boundary between metaluminous and peraluminous; *b*, Zr versus 10,000Ga/Al discrimination diagram showing that the intermediate and felsic subgroups from the BLIC are A-type granites (after Whalen et al. 1987); *c*, Nb-Y-Ce discrimination diagram indicating A_1 characteristics of the intermediate and felsic subgroups in the BLIC (after Eby 1992). Symbols are as in figure 4. The five syenite dike samples reported by Yang et al. (2007) are also plotted (*open squares*), indicating their similar major- and trace-element compositions and suggesting a magma source in common with rocks analyzed in this study.

area), the parental magma of the BLIC must be from a mantle source, and the continuous lithological and chemical variations from ultramafic-mafic through intermediate to felsic were most likely caused by crystal fractionation and accumulation (fig. 5). To determine the compositions of the primary magma, we must take the following geochemical characteristics of the BLIC into account. (1) The enrichment of the LILEs and HFSEs and the steep REE patterns indicate that the BLIC rocks could not have been produced by any crystal fractionation from a parent magma depleted in these elements. The enrichment was also unlikely to be due to crustal assimilation because the REE abundances in the studied rocks are higher than those in normal crustal materials, and adding such material would actually diminish the REE contents of the rocks (Rudnick and Gao 2003). Moreover, the whole-rock Sr-Nd isotopic compositions do not show any mixing relationship (fig. 7). Hence, the enrichment of the LILEs, HFSEs, and REEs is most likely a characteristic of the primitive magma. (2) In contrast to the enrichment of LILEs and LREEs relative to HFSEs and heavy REEs (HREEs), respectively, positive $\varepsilon Nd(t)$ values (>2.0), low $(^{87}Sr/^{86}Sr)_i$ ratios (0.70352–0.70444) of the least contaminated samples, and positive zircon $\varepsilon Hf(t)$ values (5.8–8.9) indicate a mantle source that was depleted relative to the bulk Earth, though less depleted than the N-type mid-ocean ridge basalt (MORB) source (Sun and McDonough 1989). This type of mantle source is similar to those of many oceanic and continental alkaline primary suites having positive $\varepsilon Nd(t)$ in association with LREE enrichments relative to depleted-MORB-mantle–derived rocks (N-MORB; Wedepohl and Baumann 1999). (3) The sodic alkali characteristics in major-element compositions and high Nb/Y ratios argue for sodic alkaline, or transitional (between tholeiitic and alkaline), characteristics of the primary magma (Zhao et al. 1995). (4) The BLIC intermediate syenites show geochemical characteristics similar to those of intraplate- and hotspot-related syenites, rather than those of orogenic syenites (e.g., Zhao et al. 1995).

Jiang et al. (2004*a*) and Yang et al. (2007) recently reported geochemical data of the coeval diabase and syenite dikes in the Bachu area. Although most mafic dikes are chemically evolved, they are geochemically and isotopically similar to the BLIC mafic rocks (figs. 7–9). Among the 15 analyzed mafic-dike samples reported by Jiang et al. (2004*a*), composition of diabase sample W13 (table A2) is close to that of the primary magma because (1) it is relatively high in Cr (437 ppm), Ni (246 ppm), and Mg# (54); (2) there is no Nb, Ta, P, Ti, or Sr

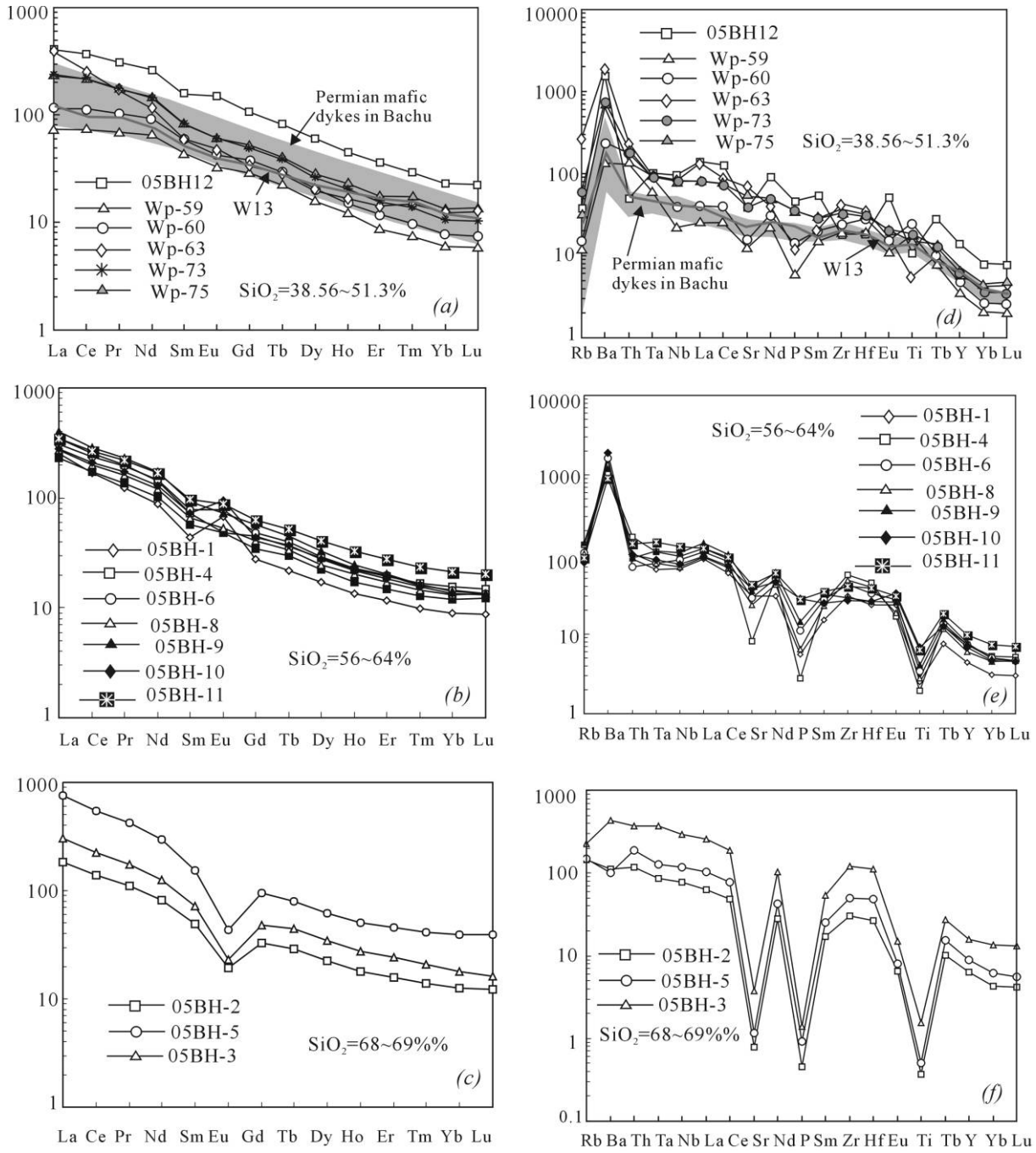

Figure 7. Chondrite-normalized rare earth element patterns (*a–c*) and primitive mantle–normalized incompatible-element spidergrams (*d–f*) for the rocks of different SiO_2 contents (in three subgroups). Data of the coeval mafic dikes from the same area are also shown (data from Jiang et al. 2004*a*), and the normalization values are from Sun and McDonough (1989).

depletion on the trace-element spidergram and no Eu anomaly on the REE pattern, indicating inappreciable crustal material contamination (fig. 9); (3) it has $\varepsilon Nd(t)$ (3.2) and $(^{87}Sr/^{86}Sr)_i$ (0.7046) comparable with those of the rocks from the BLIC; and (4) cumulative minerals are not visible in thin section (Jiang et al. 2004*a*). The Bachu mafic dikes (Jiang et al. 2004*a*) and the BLIC mafic rocks (this study) share common ocean island basalt (OIB)-like geochemical signatures, suggesting that they were

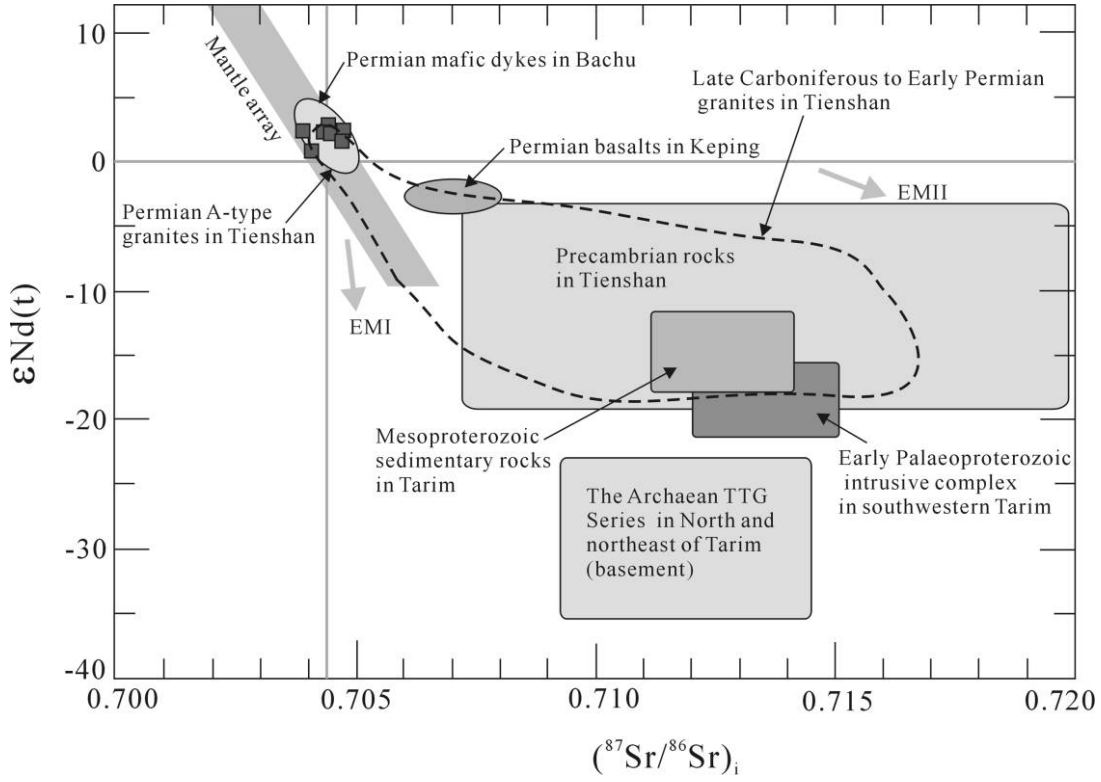

Figure 8. Sr and Nd isotopic data from the Bachu intrusive complex compared with those of various Late Carboniferous to Permian igneous rocks from the Tarim and its marginal areas (Jiang et al. 2001, 2004*a*, 2004*b*; Xu et al. 2005). Also plotted are the Precambrian basements of Tienshan and the Tarim Block (Hu et al. 1999; Xu et al. 2005; Zhang et al. 2007).

likely derived from a common OIB-like mantle source.

Crystal Fractionation and Cumulation Effects. In discussion of the crystal fractionation and cumulation effects, for convenience, we divide the magma evolution into two stages: from the "primitive magma" (W13) to the intermediate subgroup (the first stage) and from the intermediate to the silicic subgroup (the second stage), although the magma evolution was continuous. During the first stage, Fe_2O_3, CaO, and TiO_2 decreased, whereas SiO_2, K_2O, Al_2O_3, Sr, Zr, La, and Nd/P_2O_5 increased, as MgO decreased (fig. 5*a*–5*f*, 5*h*; fig. 10*d*, 10*h*, 10*f*). The variations in Ce/Sr were insignificant as MgO decreased (fig. 10*c*). Such variations are consistent with crystal fractionation of mafic minerals such as olivine, clinopyroxene, and accessory minerals, including magnetite, apatite, and titanite. However, plagioclase, alkaline feldspar (e.g., potassic feldspar), zircon, and allanite were not involved in crystallization. Covariations between Cr and Ni, Sr and Rb/Sr, and Ba and δEu also indicate that fractionation of the mafic minerals, not plagioclase, was dominant during the early stage of the magma evolution (fig. 10*a*, 10*b*, 10*e*, 10*f*). During that stage, the fractionated mafic minerals, apatite, and titanite cumulated to form the BLIC cumulate rocks (such as samples Wp-59, 60, and 73). On the other hand, fractionation of those minerals made the residue magma become more siliceous.

During the second stage, that is, from the intermediate subgroup to the silicic subgroup, as MgO decreased, Fe_2O_3 and CaO decreased, while SiO_2 and K_2O increased (fig. 5*a*–5*c*, 5*e*, 5*f*) and Cr remained roughly constant (fig. 5*g*). Such covariations suggest that crystal fractionation during the second stage was dominated by Ca-bearing mafic minerals, such as clinopyroxene and hornblende. The decreases in TiO_2, P_2O_5, and Nd/P_2O_5 and the increasing depletion of Ti and P, as shown in the trace-element spidergram, during magma evolution suggest that apatite and titanite were important fractionating phases (fig. 5*c*, 5*k*, 5*m*; figs. 7*e*, 10*g*). In contrast with the first stage, as MgO decreased, Al_2O_3 and Sr decreased (fig. 5*d*, 5*h*). Such variations, in combination with the increasing Rb/Sr ratios

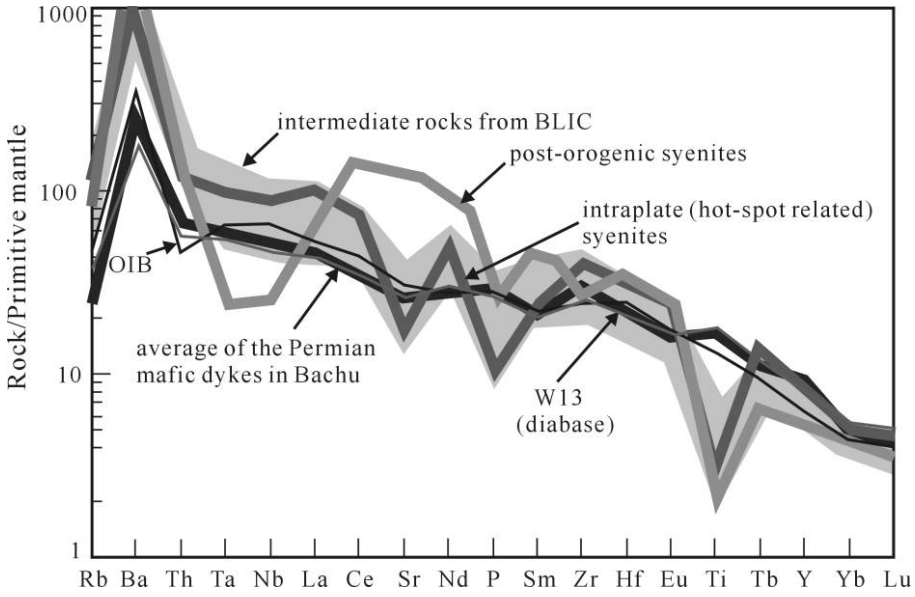

Figure 9. Comparison of the primitive mantle–normalized multielement distribution patterns between the least evolved mafic dike sample (W13) from the Bachu area and the ocean island basalt. Also plotted are alkaline rocks from rift/hotspot-related tectonic settings (McDonough et al. 1985; Baker 1987; Fisk et al. 1988) and alkaline rocks from subduction zone settings (Zhao et al. 1995; Yang et al. 2005*a*). The normalized values are from Sun and McDonough (1989). See detailed discussions in "Trace-Element and Isotopic Constraints on the Source Region."

and negative Eu anomalies during the evolution of magma from intermediate to silicic (fig. 10*b*, 10*d*, 10*e*), suggest that plagioclase fractionation was predominant. Sr and Ba decreased coherently, probably controlled by the potassic feldspar fractionation (fig. 10*b*; Jung et al. 2007). However, K_2O contents increased steadily as the magma evolved, inconsistent with potassic feldspar fractionation. Hence, the decreases in Sr and Ba were possibly controlled by the fractionation of biotite and plagioclase, which is consistent with thin-section observations (e.g., biotite was observed in both the intermediate and silicic subgroups).

It is noticeable that intermediate samples 05BH-1, 6, and 10 had significant positive Eu anomalies, which could be the result of the cumulation of the plagioclase in these samples. Thus, we suggest that there was plagioclase fractionation/unmixing in the intermediate samples.

During the second stage, allanite fractionation could have played an important role, as evidenced by Ce/Sr versus MgO and CaO versus La variations (fig. 10*c*, 10*d*). Limited Zr variations restricted the involvement of zircon crystallization among the intermediate samples. Nevertheless, in the silicic subgroup, a zircon fractionation/unmixing effect could have led to the highest Zr contents in sample 05BH-3. Furthermore, allanite fractionation/unmixing could account for the highest REE and Y contents in this sample (05BH-3), because if only zircon was involved, the sample should have had left-sloped REE distribution patterns because of the high HREE partition coefficients of the zircon.

Figure 11 illustrates our interpreted sequence of rock formation and accessory-mineral crystallization. Major- and trace-element trends can be explained by the switches from magnetite-, clinopyroxene-, and olivine-dominated crystallization and cumulation (controlling the evolution of the cumulate rocks) to biotite-, hornblende-, pyroxene-, and plagioclase-dominated crystallization and accessory minerals (such as apatite, allanite, titanite, and zircon) that controlled the intermediate-felsic subgroup trend, that is, A-type granites.

Tectonic Interpretation: A Permian Bachu LIP?

The systematic alkali characteristics and OIB-like asthenospheric mantle source for the BLIC in western Tarim suggest an extensional setting for its intrusion. Trace-element distribution patterns of the rocks from BLIC share similarities with those of alkali rocks in rift/hotspot-related tectonic settings (fig. 9; McDonough et al. 1985; Baker 1987; Fisk et al. 1988; Zhao et al. 1995; Upadhyay et al. 2006*a*, 2006*b*) but are significantly different from those of

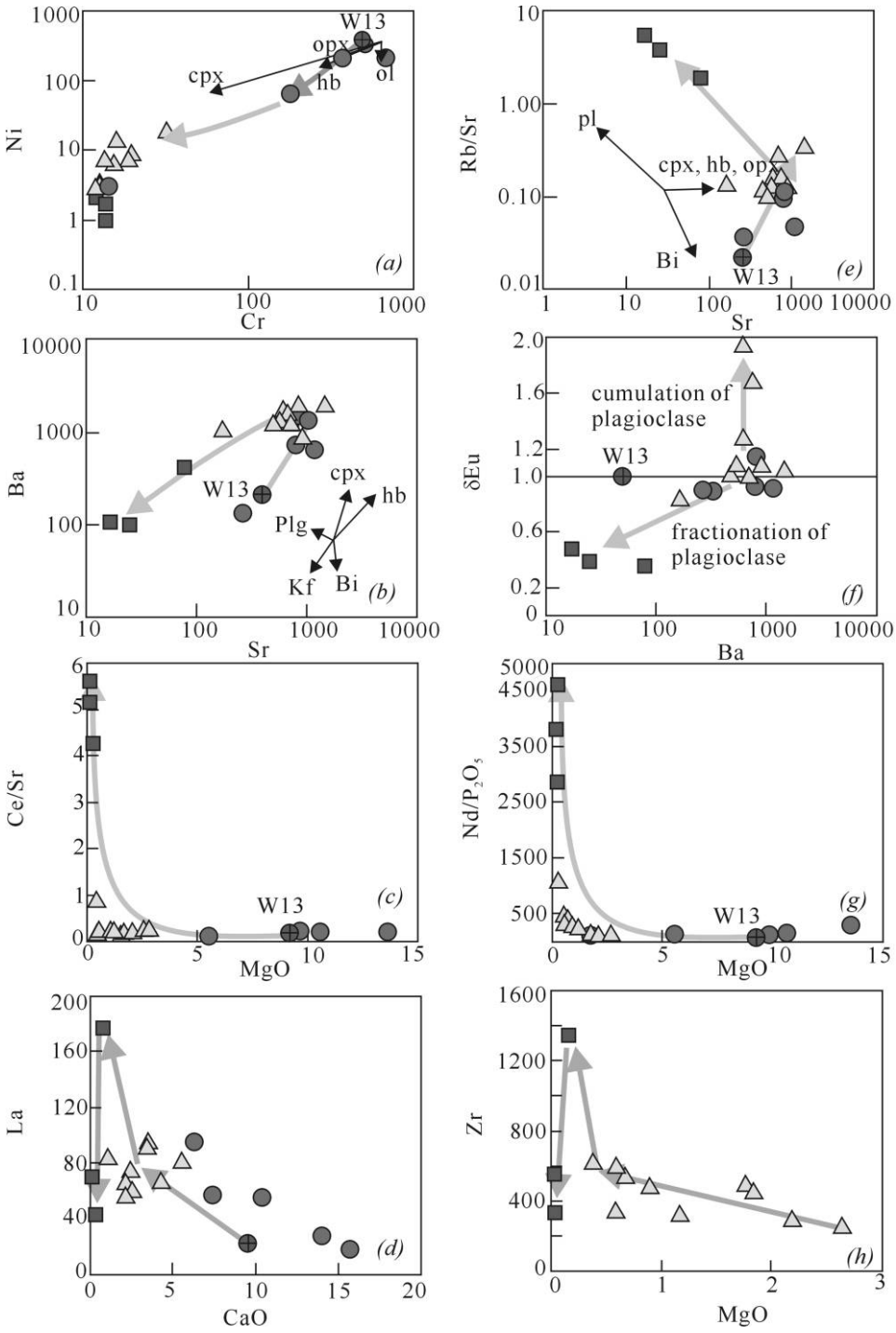

Figure 10. Binary Harker diagrams (Cr vs. Ni, Sr vs. Ba, MgO vs. Ce/Sr, CaO vs. La, Sr vs. Rb/Sr, Ba vs. δEu, MgO vs. Nd/P_2O_5, and MgO vs. Zr) for rocks of the Bachu intrusive complex, northwestern China, suggesting crystal fractionation (partition coefficients are from Rollinson 1993; see details in "Crystal Fractionation and Cumulation Effects"). Symbols are the same as in figure 4.

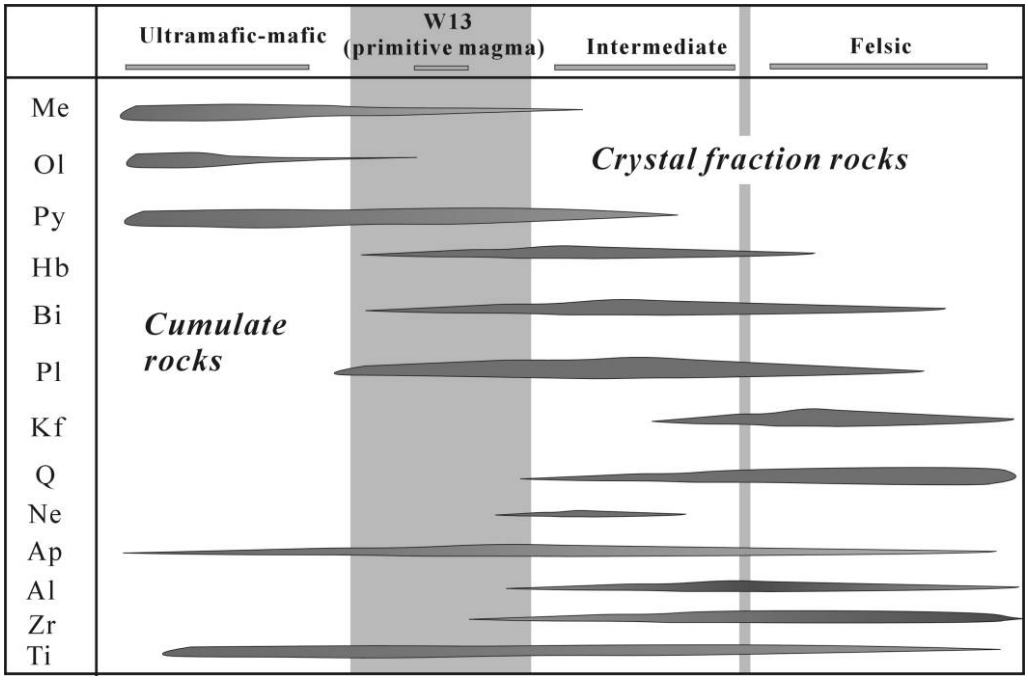

Figure 11. Mineral crystallization sequence in the different subgroups of the Bachu layered intrusive complex. *Me* = magnetite (minor titanic magnetite possibly included), *Ol* = olivine, *Py* = pyroxene, *Hb* = hornblende, *Bi* = biotite, *Pl* = plagioclase, *Kf* = potassic feldspar, *Q* = quartz, *Ne* = nepheline, *Ap* = apatite, *Al* = allanite, *Zr* = zircon, *Ti* = titanite.

subduction-zone settings (Zhao et al. 1995; Yang et al. 2005*b*). As the Tarim Block had amalgamated to the CAOB in the Late Carboniferous (Shu et al. 2000; Xia et al. 2003; Zhou et al. 2004; Li 2006), the BLIC (this study) and the coeval mafic dikes (Jiang et al. 2004*a*), bimodal dikes (Yang et al. 2006*a*), and basalts (Jiang et al. 2004*b*) in Tarim were all formed in an intracontinental extensional environment. However, it is still unclear what caused such a large-scale partial melting of the asthenospheric mantle. Several models have been proposed, including postorogenic collapse (Xu et al. 2005; Zhou et al. 2006), a mantle plume (Zhou et al. 2004), and paleo-Tethyan subduction north of the Qinghai-Tibet Plateau (Yang et al. 1995, 2005*b*, 2006*a*). The following observations led us to conclude that the large-scale Permian igneous events in Tarim and its surrounding regions were results of a mantle plume breakout.

1. *The large volume of the Permian mafic igneous rock in Tarim*. Recent geochronological and stratigraphic (especially detailed paleontology) studies on the Permian basalts in Tarim and its marginal areas show that a large volume of basalts erupted between 280 and 270 Ma (figs. 12, 13; Chen et al. 1997, 2006; Jia et al. 2004; Jiang et al. 2001,

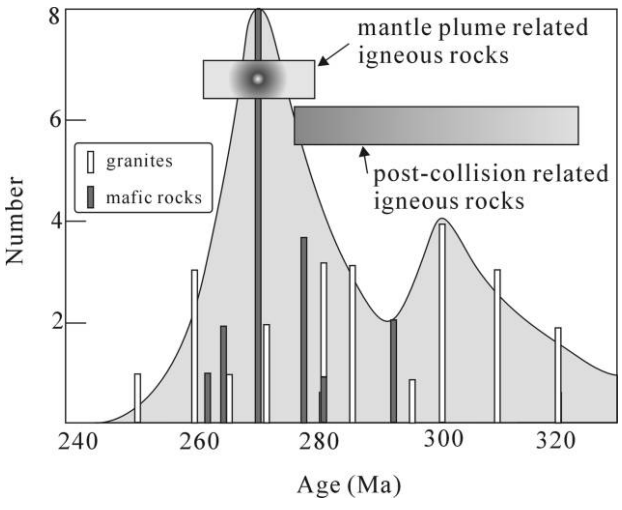

Figure 12. Cumulative age spectra of the Late Carboniferous to Permian igneous rocks in Tarim and its marginal areas. The age data are from Chen et al. (1997), Jia (1997), Gu et al. (2001), Jiang et al. (2004*a*), Zhou et al. (2004, 2006), Xu et al. (2005), Zhang et al. (2005), Yang et al. (2006*a*), and this study. The ages included both zircon SHRIMP U-Pb ages and whole-rock Ar-Ar plateau ages (for basalts).

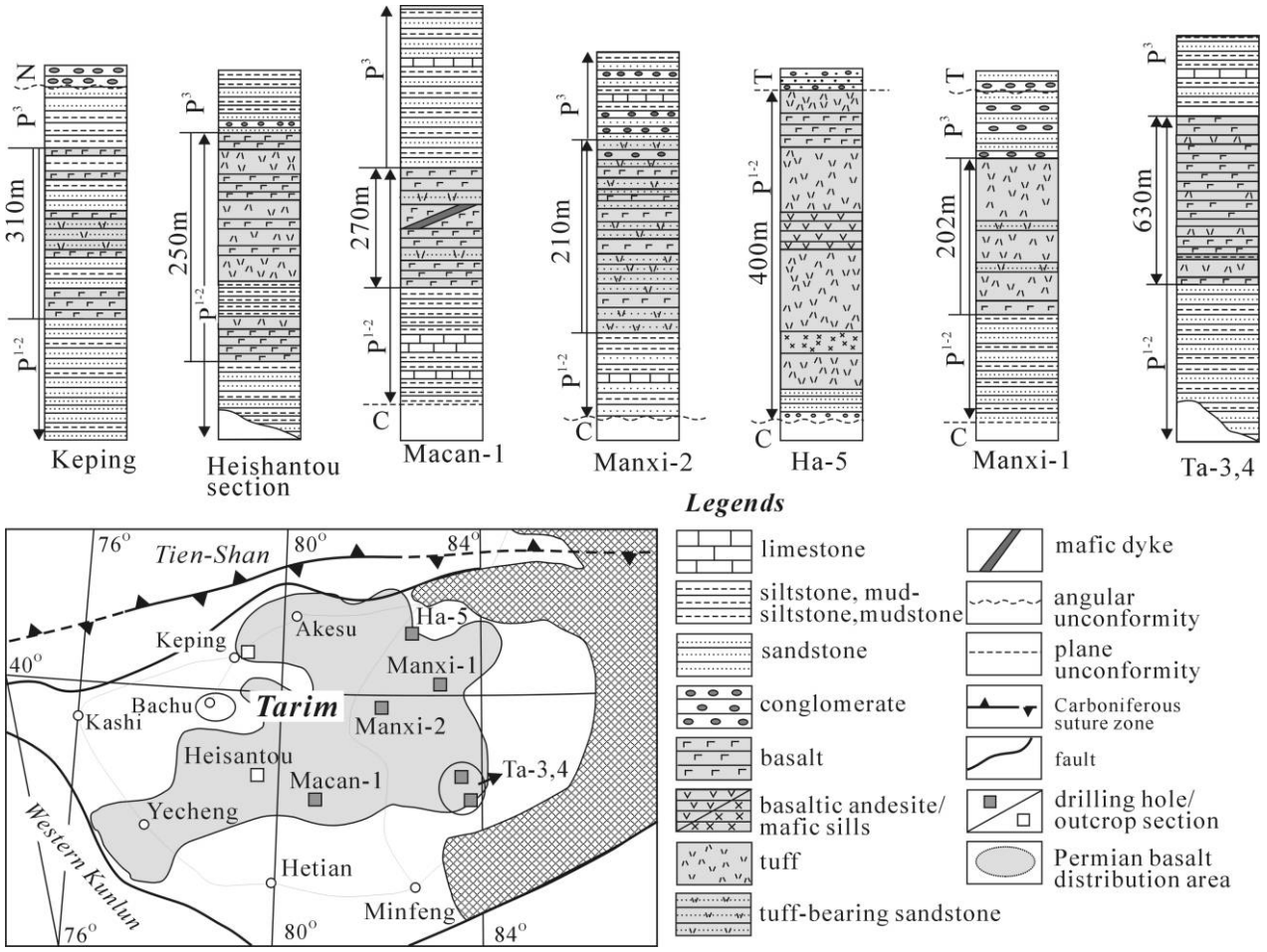

Figure 13. Stratigraphic positions and thicknesses of the Permian basalts in Tarim (original data from Jia et al. 2004; Jiang et al. 2004*b*).

2004*a*, 2004*b*; Zhou et al. 2006). According to geophysical exploration and drill-hole data (Jia 1997; Chen et al. 2006), the area coverage of the Permian basalts (including related tuff and tuff-bearing rocks) in Tarim is ca. 250,000 km^2. Drill-hole and section data (Jia et al. 2004; Chen et al. 2006) indicate that the thickness of the basalts varies between ~100 and ~800 m, with an estimated average thickness of ca. 300 m based on the published drill-hole and section data (fig. 13; Jia et al. 2004; Jiang et al. 2004*b*). Thus, the volume of the Permian basalts in Tarim is estimated at ca. 75,000 km^3. If the coeval basalts in the Tuha and Sangtanghu basins north of Tienshan (fig. 1*a*; Zhou et al. 2006) and the widely distributed Permian mafic dikes in Tarim (Zhang et al. 1998; Jiang et al. 2004*b*) are included, the total volume of the basaltic rocks could be up to 100,000 km^3.

2. *Different magma sources for the coeval Permian mafic rocks.* Geochemical data indicate that the coeval mafic rocks at different locations were derived from different mantle sources (Zhang et al. 1998; Jiang et al. 2004*b*; Zhou et al. 2004, 2006; this study). For example, the basalts in Tarim (samples were from the Keping area and several drill holes in Tarim) have both negative $\varepsilon Nd(t)$ (-2 to -5) and high Nb/La ratios (1.0–1.2), indicating that they were derived from a long-term enriched lithospheric mantle source (Rui et al. 2002, p. 29–47; Jiang et al. 2004*b*; Yang et al. 2005*b*); the basalts north of Tienshan (the Tuha and Sangtanghu basins) were likely derived from partial melting of a lithospheric mantle previously metasomatized by subduction materials in an extensional regime (fig. 1*a*; Zhou et al. 2006); the mafic intrusions in the Huangshan district of eastern Tienshan and the mafic dikes in eastern Tienshan were likely sourced from a lithospheric mantle that was pre-

viously contaminated by subducting oceanic crust (Zhang et al. 1998; Zhou et al. 2004). More important, the estimated primary magma of the Huangshan intrusion had a high Mg# of up to 73, indicating a high melting temperature (Zhou et al. 2004).

3. *Voluminous Permian A-type granites and cooling events in Tienshan.* Voluminous Permian A-type granites in the CAOB, coeval with mafic extrusions/intrusions in Tarim and its northern marginal areas, have positive $\varepsilon Nd(t)$ values indicating a direct or (more likely) indirect mantle contribution, suggesting an indirect genetic link between the mafic-ultramafic intrusions and the A-type granitic plutons in Tienshan (Jahn et al. 2000*a*). Permian thermal events have also been identified within the CAOB. For example, Shu et al. (2000) reported $^{40}Ar/^{39}Ar$ ages of 269 Ma for muscovite and 281 Ma for biotite in a deformed granite in the 470-Ma Weiya granite intrusion in eastern Tienshan.

4. *Permian crustal doming in Tarim*. Because most of Tarim was covered by desert, it is difficult to reconstruct detailed Carboniferous to Permian lithofacies paleogeography for it. However, on the basis of studies from the drill holes in the interior of the basin and several outcrops along its marginal area (Jia et al. 2004), Chen et al. (2006) suggested that from the late Cisuralina to the Guadalupian epoch, there was a remarkable crustal doming event in Tarim and that the doming might have been centered in the Bachu area. This crustal doming event coincided with basaltic eruptions in Tarim, mainly between the Cisuralina and Guadalupian epochs (e.g., an Ar-Ar plateau age of 278.5 ± 1.5 Ma for basalts in central Tarim; see "U-Pb Zircon Age").

On the basis of the above analyses, we question the interpretation that the voluminous mafic volcanic rocks in Tarim were genetically related to the paleo-Tethyan subduction north of the Qinghai-Tibet Plateau (Yang et al. 2005*b*, 2006*a*). Regional geology also argues against this model. For example, (1) although the dating is still debatable, Tarim appears to have amalgamated with the CAOB by the Late Carboniferous (Shu et al. 2000; Zhou et al. 2004; Li 2006); (2) recent studies indicate that the north-dipping subduction along the south margin of the southern Kunlun Terrane (the Kangxiwa suture zone) lasted from at least the mid-Carboniferous to the Early Triassic (Xiao et al. 2002, 2005; Zhang et al. 2007), and if the voluminous basalts and the BLIC were genetically related to the subduction, the igneous activities should have lasted from the Carboniferous to the Triassic rather than being a short pulse, as observed in Tarim (fig. 12). The postcollisional delamination model for the Tienshan orogenic belt could properly explain the Late Carboniferous to Early Permian (320–290 Ma) granitic rocks there and the minor basalts dated at ~290 Ma north of Tienshan (fig. 12; Gu et al. 2000, 2006; Xu et al. 2005; Zhou et al. 2006), similar to the formation of the voluminous Mesozoic granites and minor mafic rocks in South China (Li and Li 2007). However, it is unlikely that the delamination of subducted slab could have induced the large volume of ca. 270-Ma mafic rocks in Tarim.

We suggest that the coeval voluminous, variably sourced mafic rocks in Tarim and its marginal area, as well as the several mafic intrusions and voluminous A-type granites in Tienshan, constitute a Permian large igneous province in northwestern China, which we term "the Bachu LIP." The ca. 274-Ma BLIC at Bachu is possibly a residue feeder of the voluminous basalts in Tarim. If the Bachu LIP was the product of a ca. 275-Ma mantle plume, it possibly began at ca. 285–280 Ma and reached kurtosis at ca. 275 Ma (fig. 12; Borisenko et al. 2006), and moreover, it would have occurred ca. 20 m.yr. before the well known Emeishan LIP in southwestern China (Zhou et al. 2002; Xu et al. 2004) and 25 m.yr. before the 251-Ma Siberian Traps in Russia (Campbell et al. 1992; Pisarevsky et al. 2006). Such a sudden flare-up of plume activities in the Permian may represent the early stage of the dipolar Pangaea and southwest-Pacific superplumes due to circum-Pangaea subduction and mantle avalanches (Li et al. 2008).

Conclusions

Using new data acquired during this study, as well as existing information about Permian magmatic activities in Tarim and surrounding regions, we draw the following conclusions. (1) The Bachu alkaline ultramafic-mafic-felsic layered intrusive complex (BLIC) is a typical layered intrusion emplaced at ca. 274 Ma in the interior of the Tarim Block. Elemental and whole-rock Sr-Nd isotope compositions and zircon Hf isotope data argue that the BLIC was formed via crystal cumulation and fractionation (with minor crustal contamination) of alkali basalt derived from an OIB-like asthenospheric mantle source. (2) The BLIC, coeval voluminous basalts in Tarim, and mafic and A-type intrusions around Tarim constitute an LIP (which we term the Permian Bachu LIP). This LIP was likely the result of a Permian (ca. 275-Ma) mantle plume under Tarim, and the BLIC could be the residue of a feeder for this Permian LIP.

ACKNOWLEDGMENTS

We thank Y. Liu and X. Liang for helping with major-element, trace-element, and Nd-Sr isotope analyses and X. Liu and Y. Yang for assistance with zircon LA-ICP-MS age and Hf isotope data acquisition. This work was supported by National Science Foundation of China (grants 40721063, 40772123, 40421303) and the Programme of Excellent Young Scientists of the Ministry of Land and Resources (grant to C.-L. Zhang). This is TIGeR (The Institute for Geoscience Research) publication no. 105.

REFERENCES CITED

Bailey, J. C.; Gwozdz, R.; Rose-Hansen, J., and Sørensen, H. 2001. Geochemical overview of the Ilímaussaq alkaline complex, South Greenland. Geol. Greenl. Surv. Bull. 190:35–54.

Bailey, J. C.; Sørensen, H.; Andersen, T.; Kogarko, L. N.; and Rose-Hansen, J. 2006. On the origin of microrhythmic layering in arfvedsonite lujavrite from the Ilímaussaq alkaline complex, South Greenland. Lithos 91:301–318.

Baker, B. H. 1987. Outline of the petrology of the Kenya Rift alkaline province. *In* Fitton, J. G., and Upton, B. G. J., eds. Alkaline igneous rocks. Geol. Soc. Lond. Spec. Publ. 30:293–311.

Baker, J. A.; Menzies, M. A.; Thirlwall, M. F.; and Macpherson, C. G. 1997. Petrogenesis of Quaternary intraplate volcanism, Sana'a, Yemen: implications for plume-lithosphere interaction and polybaric melt hybridization. J. Petrol. 38:1359–1390.

Black, L. P.; Kamo, S. L.; Allen, C. M.; Aleinikoff, J. N.; Davis, D. W.; Korsch, R. J.; and Foudoulis, C. 2003. TEMORA 1: a new zircon standard for Phanerozoic U-Pb geochronology. Chem. Geol. 200:155–170.

Borisenko, A. S.; Sotnikov, V. I.; Izokh, A. E.; Polyakov, G. V.; and Obolensky, A. A. 2006. Permo-Triassic mineralization in Asia and its relation to plume magmatism. Russ. Geol. Geophys. 47:166–182.

Campbell, I. H.; Czamanske, G. K.; Fedorenko, V. A.; Hill, R. I.; and Stepanov, V. 1992. Synchronism of the Siberian Traps and the Permian-Triassic boundary. Science 258:1760–1763.

Chen, H. L.; Yang, S. F.; and Dong, C. W. 1997. The discovery of early Permian basic rock belt in Tarim Basin and its tectonic meanings. Geochemica 22:77–87 (in Chinese).

———. 1999. Characteristics and geodynamics of the Early Permian igneous rocks in Tarim Basin. *In* Chen, H. H., ed. Studies on collisional orogenic belt. Beijing, Ocean Press, p. 174–182 (in Chinese).

Chen, H. L.; Yang, S. F.; Wang, Q. H.; Luo, J. C.; Jia, C. Z.; Wei, G. Q.; and Li, Z. L. 2006. Sedimentary response to the Early-mid-Permian basaltic magmatism in the Tarim plate. Geol. China 33:545–552 (in Chinese).

Chen, Y.; Xu, B.; Zhan, S.; and Li, Y. 2004. First mid-Neoproterozoic paleomagnetic results from the Tarim Basin (NW China) and their geodynamic implications. Precambrian Res. 133:271–281.

Dawson, J. B. 1987. The kimberlite clan: relationship with olivine and leucite lamproites, and inferences for upper-mantle metasomatism. *In* Fitton, J. G., and Upton, B. G. J., eds. Alkaline igneous rocks. Geol. Soc. Lond. Spec. Publ. 30:95–101.

Dorais, M. J. 1990. Compositional variations in pyroxenes and amphiboles of the Belknap Mountain complex, New Hampshire: evidence for origin of silica-saturated alkaline rocks. Am. Mineral. 75:1092–1105.

Eby, G. N. 1992. Chemical subdivision of the A-type granitoids: petrogenetic and tectonic implications. Geology 20:641–644.

Edgar, A. D. 1987. The genesis of alkaline magmas with emphasis on their source regions: inferences from experimental studies. *In* Fitton, J. G., and Upton, B. G. J., eds. Alkaline igneous rocks. Geol. Soc. Lond. Spec. Publ. 30:29–52.

Farmer, G. L. 2003. Continental basaltic rocks. *In* R. L. Rudnick, ed. The crust. Vol. 3 of Holland, H. D., and Turekian, K. K., eds. Treatise on geochemistry. Oxford, Elsevier-Pergamon, p. 85–121.

Fisk, M. R.; Upton, B. G. J.; and Ford, C. E. 1988. Geochemical and experimental study of the genesis of magma of Reunion Island, India Ocean. J. Geophys. Res. 93:4933–4950.

Fitton, J. G. 1987. The Cameroon line, west Africa: a comparison between oceanic and continental alkaline volcanism. *In* Fitton, J. G., and Upton, B. G. J., eds. Alkaline igneous rocks. Geol. Soc. Lond. Spec. Publ. 30:273–291.

Frimmel, H. E.; Zartman, R. E.; and Späth, A. 2001. The Richtersveld igneous complex, South Africa: U-Pb zircon and geochemical evidence for the beginning of Neoproterozoic continental breakup. J. Geol. 109:493–508.

Gu, L. X.; Hu, S. X.; Yu, C. S.; Wu, C. Z.; and Yan, Z. F. 2000. Carboniferous volcanites in the Bogda orogenic belt of the east Tianshan: their tectonic implications. Acta Petrol. Sin. 16:305–316 (in Chinese).

———. 2001. Initiation and evolution of the Bogda subduction-torn-type rift. Acta Petrol. Sin. 17:585–597 (in Chinese).

Gu, L. X.; Zhang, Z. Z.; Wu, C. Z.; Wang, Y. X.; Tang, J. H.; Wang, C. S.; Xi, A. H.; and Zhen, Y. C. 2006. Some problems of the granites and vertical growth of the continental crust in the eastern Tianshan Mountains, NW China. Acta Petrol. Sin. 22:1103–1120 (in Chinese with English abstract).

Hu, A. Q.; Zhang, Q. F.; Zhang, G. X.; and Chen, Y. B. 1998. Constraints on the age of basement and crustal growth in Tianshan Orogen by Nd isotope composi-

tions. Sci. China Ser. D 28:648–657 (in Chinese with English abstract).
Huang, W. L., and Wyllie, P. J. 1981. Phase relationship of S-type granite with H_2O to 35 kbar: muscovite granite from Harney Peak, South Dakota. J. Geophys. Res. 86:10,515–10,529.
Jahn, B. M.; Wu, F.; Capdevila, R.; Martineau, F.; Zhao, Z. H.; and Wang, Y. X. 2001. Highly evolved juvenile granites with tetrad REE patterns: the Woduhe and Baerzhe granites from the Great Xing'an Mountains in NE China. Lithos 59:171–198.
Jahn, B. M.; Wu, F.; and Chen, B. 2000*a*. Granitoids of the Central Asian Orogenic Belt and continental growth in the Phanerozoic. Trans. R. Soc. Edinb.: Earth Sci. 91:181–193.
Jahn, B. M.; Wu, F. Y.; and Hong, D. W. 2000*b*. Important crustal growth in the Phanerozoic: isotopic evidence of granitoids from east-central Asia. Proc. Indian Acad. Sci. Earth Planet. Sci. 109:5–20.
Jia, C. Z. 1997. Tectonic characteristics and oil-gas in the Tarim Basin, China. Beijing, Petroleum Industry Press (in Chinese).
Jia, C. Z.; Zhang, S. B.; and Wu, S. Z. 2004. Stratigraphy of the Tarim Basin and adjacent areas. Vol. 2. Beijing, Science Press, 513 p.
Jiang, C. Y.; Jia, C. Z.; Li, L. C.; Zhang, P. B.; Lu, D. R.; and Bai, K. Y. 2004*a*. Source of the Fe-enriched-type high-Mg magma in Mazhartag region, Xinjiang. Acta. Geol. Sin. 78:770–780 (in Chinese with English abstract).
Jiang, C. Y.; Wu, W. K.; Li, L. C.; Mu, Y. M.; Bai, K. Y.; and Zhao, X. L. 2001. Phanerozoic tectonic evolution of the eastern part of the southern Tienshan. Beijing, Geological Publishing House, 160 p. (in Chinese).
Jiang, C. Y.; Zhang, P. B.; Lu, D. R.; Bai, K. Y.; Wang, Y. P.; Tang, S. H.; Wang, J. H.; and Yang, C. 2004*b*. Petrology, geochemistry and petrogenesis of the Kalpin basalts and their Nd, Sr and Pb isotopic compositions. Geol. Rev. 50:492–500 (in Chinese with English abstract).
Jung, S.; Hoffer, E.; and Hoern, S. 2007. Neo-Proterozoic rift-related syenites (northern Damara Belt, Namibia): geochemical and Nd-Sr-Pb-O isotope constraints for mantle sources and petrogenesis. Lithos 96:415–435.
Li, C. N.; Lu, F. X.; and Chen, M. H. 2001. Research on petrography of the Wajilitag complex body on the north edge of the Tarim Basin. Xinjiang Geol. 19:38–42 (in Chinese).
Li, J. Y. 2006. Permian geodynamic setting of northeast China and adjacent regions: closure of the Paleo-Asian Ocean and subduction of the Paleo-Pacific Plate J. Asian Earth Sci. 26:207–224.
Li, X. H.; Li, Z. X.; Ge, W.; Zhou, H.; Li, W.; Liu, Y.; and Wingate, M. T. D. 2003. Neoproterozoic granitoids in South China: crustal melting above a mantle plume at ca. 825 Ma? Precambrian Res. 122:45–83.
Li, X. H.; Li, Z. X.; Zhou, H.; Liu, Y.; and Kinny, P. D. 2002. U-Pb zircon geochronology, geochemistry and Nd isotopic study of the Neoproterozoic biomodal volcanic rocks in the Kangdian rift of South China: implication for the initial rifting of Rodinia. Precambrian Res. 113:135–154.
Li, X. H.; Liu, D. Y.; Sun, M.; Li, W. X.; Liang, X. R.; and Liu, Y. 2004. Precise Sm-Nd and U-Pb isotopic dating of the super-giant Shizhuyuan polymetallic deposit and its host granite, southeast China. Geol. Mag. 141: 225–231.
Li, X. H.; Qi, C. S.; Liu, Y.; Liang, X. R.; Tu, X. L.; Xie, L. W.; and Yang, Y. H. 2005. Petrogenesis of the Neoproterozoic bimodal volcanic rocks along the western margin of the Yangtze Block: new constraints from Hf isotopes and Fe/Mn ratios. Chin. Sci. Bull. 50:2481–2486.
Li, Z. X.; Bogdanova, S. V.; Collins, A. S.; Davidson, A.; De Waele, B.; Ernst, R. E.; Fitzsimons, I. C. W.; et al. 2008. Assembly, configuration, and break-up history of Rodinia: a synthesis. Precambrian Res. 160:179–210.
Li, Z. X., and Li, X. H. 2007. Formation of the 1300-km-wide intracontinental orogen and postorogenic magmatic province in Mesozoic South China: a flat-slab subduction model. Geology 35:179–182.
Litvinovsky, B. A.; Jahn, B. M.; Zanvilevich, A. N.; and Shadaev, M. G. 2002. Crystal fractionation in the petrogenesis of an alkali monzodiorite-syenite series: the Oshurkovo plutonic sheeted complex, Transbaikalia, Russia. Lithos 64:97–130.
Lubala, R. T.; Frick, C.; Roders, J. H.; and Walraven, F. 1994. Petrogenesis of syenites and granites of the Schiel alkaline complex, North Transvaal, South Africa. J. Geol. 102:307–309.
Ludwig, K. R. 2003. Isoplot 3.0: a geochronological toolkit for Microsoft Excel. Berkeley, CA, Berkeley Geochronol. Cent. Spec. Publ. 4.
Martin, R. F. 2006. A-type granites of crustal origin ultimately result from open-system fenitization-type reactions in an extensional environment. Lithos 91:125–136.
McDonough, W. F.; McCulloch, M. T.; and Sun, S. S. 1985. Isotopic and geochemical systematic in Tertiary-Recent basalts from southeastern Australia and implications for the evolution of the sub-continental lithosphere. Geochim. Cosmochim. Acta 49:2051–2067.
Menzies, M. 1987. Alkaline rocks and their inclusions: a window on the Earth's interior. *In* Fitton, J. G., and Upton, B. G. J., eds. Alkaline igneous rocks. Geol. Soc. Lond. Spec. Publ. 30:15–27.
Pisarevsky, S. A.; Gladkochub, D. P.; Donskaya, T. A.; De Waele, B.; and Mazukabzov, A. M. 2006. Palaeomagnetism and geochronology of mafic dykes in south Siberia, Russia: the first precisely dated Early Permian palaeomagnetic pole from the Siberian craton. Geophys. J. Int. 167:649–658.
Rollinson, H. R. 1993. Using geochemical data: evaluation, presentation, interpretation. Singapore, Longmans.
Rudnick, R. L., and Gao, S. 2003. Composition of the continental crust. *In* Rudnick, R. L., ed. The crust. Vol. 3 of Holland, H. D., and Turekian, K. K., eds.

Treatise on geochemistry. Oxford, Elsevier-Pergamon, p. 1–64.

Rui, X. J.; He, J. R.; and Guo, K. Y. 2002. Mineral resources of Tarim Block. Beijing, Geological Publishing House (in Chinese).

Shu, L. S.; Chen, Y.; Lu, H.; Charvet, J.; Laurent, S.; and Yin, D. 2000. Paleozoic accretionary terranes in northern Tianshan, NW China. Chin. J. Geochem. 19:193–202.

Sun, S. S., and McDonough, W. F. 1989. Chemical and isotopic systematics of oceanic basalts: implications for mantle composition and processes. *In* Saunders, A. D., and Norry, M. J., eds. Magmatism in the ocean basin. Geol. Soc. Lond. Spec. Publ. 42:313–345.

Upadhyay, D.; Jahn-Awe, S.; Pin, C.; Paquette, J. L.; and Braun, I. 2006*a*. Neoproterozoic alkaline magmatism at Sivamalai, southern India. Gondwana Res. 10:156–166.

Upadhyay, D.; Raith, M. M.; Mezger, K.; and Hammerschmidt, K. 2006*b*. Mesoproterozoic rift-related alkaline magmatism at Elchuru, Prakasam Alkaline Province, SE India. Lithos 89:447–477.

Wedepohl, K. H., and Baumann, A. 1999. Central European Cenozoic plume volcanism with OIB characteristics and indications of a lower mantle source. Contrib. Mineral. Petrol. 136:225–239.

Whalen, J. B.; Currie, K. L.; and Chappell, B. W. 1987. A-type granites: geochemical characteristics, discrimination and petrogenesis. Contrib. Mineral. Petrol. 95: 407–419.

Wiedenbeck, M.; Alle, P.; Corfu, F.; Griffin, W. L.; Meier, F.; Oberli, F.; Von Quadt, A.; Roddick, J. C.; and Spiegel, W. 1995. Three natural zircon standards for U-Th-Pb; Lu-Hf, trace element, and REE analyses. Geostand. Newsl. 19:1–23.

Winchester, J. A., and Floyd, P. A. 1977. Geochemical discrimination of different magma series and their differentiation products using immobile elements. Chem. Geol. 20:325–343.

Wu, F. Y.; Yang, J. H.; Wilde, S. A.; and Zhang, X. O. 2005. Geochronology, petrogenesis and tectonic implications of the Jurassic granites in the Liaodong Peninsula, NE China. Chem. Geol. 221:127–156.

Wu, F. Y.; Yang, Y. H.; Xie, L. W.; Yang, J. H.; and Xu, P. 2006. Hf isotopic compositions of the standard zircons and baddeleyites used in U-Pb geochronology. Chem. Geol. 234:105–126.

Xia, L. Q.; Xu, X. Y.; and Xia, Z. C. 2003. Carboniferous post-collisional rift volcanic rocks in the Tianshan Mountains, northwestern China. Acta Geol. Sin. 77: 338–360.

Xiao, W. J.; Windley, B. F.; and Chen, H. L. 2002. Carboniferous-Triassic subduction and accretion in the western Kunlun, China: implications for the collisional and accretionary tectonics of the northern Tibet plateau. Geology 30:295–298.

Xiao, W. J.; Windley, B. F.; and Liu, D. Y. 2005. Accretionary tectonics of the Western Kunlun Orogen, China: a Paleozoic–early Mesozoic, long-lived active continental margin with implications for the growth of southern Eurasia. J. Geol. 113:687–705.

Xinjiang BGMR (Bureau of Geology and Mineral Resources). 1993. Regional geology of the Xinjiang Uygur Autonomous Region. Beijing, Geological Publishing House (in Chinese).

Xu, X. Y.; Ma, Z. P.; Xia, Z. C.; Xia, L. Q.; Li, X. M.; and Wang, L. S. 2005. Discussion of the sources and characteristics on Sr, Nd, Pb isotopes of the Carboniferous to Permian post-collision granites from Tienshan. Northwest. Geol. 38:1–18 (in Chinese with English abstract).

Xu, Y. G.; He, B.; Chung, S.-L.; Menzies, M. A.; and Frey, F. A. 2004. Geological, geochemical and geophysical consequences of plume involvement in the Emeishan flood-basalt province. Geology 32:917–920.

Yang, J. H.; Chung, S. L.; Wilde, S. A.; Wu, F. Y.; Chu, M. F.; Lo, C. H.; and Fan, H. R. 2005*a*. Petrogenesis of post-orogenic syenites in the Sulu Orogenic Belt, East China: geochronological, geochemical and Nd-Sr isotopic evidence. Chem. Geol. 214:99–125.

Yang, S. F.; Chen, H. L.; and Dong, C. W. 1995. The discovery of the Permian syenite inside the Tarim Basin and its geodynamic significance. Geochemica 25:121–128 (in Chinese).

Yang, S. F.; Chen, H. L.; Ji, D. W.; Li, Z. L.; Dong, C. W.; Jia, C. Z.; and Wei, G. Q. 2005*b*. Geological process of early to middle Permian magmatism in Tarim Basin and its geodynamic significance. Geol. J. China Univ. 11:504–511 (in Chinese).

Yang, S. F.; Li, Z.; Chen, H.; Santosh, M.; Dong, C. W.; and Yu, X. 2007. Permian bimodal dyke of Tarim Basin, NW China: geochemical characteristics and tectonic implications. Gondwana Res. 12:113–120.

Yang, S. F.; Li, Z. L.; Chen, H. L.; Xiao, W. J.; Yu, X.; Lin, X. W.; and Shi, X. G. 2006*a*. Discovery of a Permian quartz syenite porphyritic dyke from the Tarim Basin and its tectonic implications. Acta Petrol. Sin. 22: 1405–1412 (in Chinese).

Yang, Y. H.; Zhang, H. F.; Xie, L. W.; Liu, Y.; Qi, C. S.; and Tu, X. L. 2006*b*. Petrogenesis of typical Mesozoic and Cenozoic volcanic rocks from the North China Craton: new evidence from Hf isotope studies. Acta Geol. Sin. 22:1566–1576 (in Chinese).

Yuan, H. L.; Gao, S.; Liu, X. M.; Li, H. M.; Günther, D.; and Wu, F. Y. 2004. Accurate U-Pb age and trace element determinations of zircon by laser ablation-inductively coupled plasma mass spectrometry. Geostand. Geoanal. Res. 28:353–370.

Zhang, C. L.; Lu, S. N.; Yu, H. F.; and Ye, H. M. 2007. Tectonic evolution of the western Kunlun orogenic belt in northern Qinghai-Tibet Plateau: evidence from zircon SHRIMP and LA-ICP-MS U-Pb geochronology. Sci. China Ser. D 50:825–835.

Zhang, Z. C.; Guo, Z. J.; and Liu, S. W. 1998. Age and tectonic significance of the mafic dyke swarm in the Kuruketag region, Xinjiang. Acta Geol. Sin. 72:29–36.

Zhang, Z. Z.; Gu, L. X.; Wu, C. Z.; San, J. Z.; Tang, J. H.; Xi, A. H.; and Wang, S. 2005. Weiya complex, eastern

Tianshan: single sourced or diverse sourced? evidence from biotite. Geochemica 34:328–338 (in Chinese).

Zhao, J. X.; Shiraishi, K.; Ellis, D. J.; and Sheraton, J. W. 1995. Geochemical and isotopic studies of syenites from the Yamato Mountains, East Antartica: implications for the origin of syenitic magmas. Geochim. Cosmochim. Acta 59:1363–1385.

Zhou, D. W.; Liu, Y. Q.; Xin, X. J.; Hao, J. R.; Dong, Y. P.; and Ouyang, Z. J. 2006. Formation of the Permian basalts and implications of geochemical tracing for paleo-tectonic setting and regional tectonic background in the Turpan-Hami and Santanghu basins, Xinjiang. Sci. China Ser. D 49:584–596.

Zhou, M. F.; Lesher, C. M.; Yang, Z. X.; Li. J. W.; and Sun, M. 2004. Geochemistry and petrogenesis of 270 Ma Ni-Cu-(PGE) sulfide-bearing mafic intrusions in the Huangshan district, eastern Xinjiang, northwest China: implications for the tectonic evolution of the Central Asian orogenic belt. Chem. Geol. 209:233–257.

Zhou, M. F.; Malpas, J.; Song, X.; Kennedy, A. K.; Robinson, P. T.; Sun, M.; Lesher, M.; and Keays, R. R. 2002. A temporal link between the Emeishan large igneous province (SW China) and the end-Guadalupian mass extinction. Earth Planet. Sci. Lett. 196:113–122.